communications biology

Article

https://doi.org/10.1038/s42003-024-06665-w

Transcriptomic decoding of regional cortical vulnerability to major depressive disorder

Jiajia Zhu[1,2,3], Xiao Chen[4,5,6,7], Bin Lu[4,5,6,7], Xue-Ying Li[4,5,6,7], Zi-Han Wang[4,5,6,7], Li-Ping Cao[8], Guan-Mao Chen[9], Jian-Shan Chen[8], Tao Chen[10], Tao-Lin Chen[11,12], Yu-Qi Cheng[13], Zhao-Song Chu[13], Shi-Xian Cui[4,14,15], Xi-Long Cui[16], Zhao-Yu Deng[4,5,6,7], Qi-Yong Gong[11,12], Wen-Bin Guo[16], Can-Can He[17], Zheng-Jia-Yi Hu[4,14,15], Qian Huang[18], Xin-Lei Ji[16], Feng-Nan Jia[19], Li Kuang[18], Bao-Juan Li[20], Feng Li[21], Hui-Xian Li[4,5,6,7], Tao Li[22,23], Tao Lian[4,5,6], Yi-Fan Liao[4,5,6], Xiao-Yun Liu[24], Yan-Song Liu[19], Zhe-Ning Liu[16], Yi-Cheng Long[16], Jian-Ping Lu[25], Jiang Qiu[26], Xiao-Xiao Shan[16], Tian-Mei Si[27], Peng-Feng Sun[28], Chuan-Yue Wang[21], Hua-Ning Wang[20], Xiang Wang[16], Ying Wang[9], Yu-Wei Wang[4,5,6,7], Xiao-Ping Wu[28], Xin-Ran Wu[26], Yan-Kun Wu[27], Chun-Ming Xie[17], Guang-Rong Xie[16], Peng Xie[29,30,31], Xiu-Feng Xu[13], Zhen-Peng Xue[25], Hong Yang[10], Hua Yu[22,23], Min-Lan Yuan[32], Yong-Gui Yuan[24], Ai-Xia Zhang[33], Jing-Ping Zhao[16], Ke-Rang Zhang[33], Wei Zhang[32], Zi-Jing Zhang[4,5,6], Chao-Gan Yan[4,5,6,7,14,15], the DIRECT Consortium* & Yongqiang Yu[1,2,3] ✉

Previous studies in small samples have identified inconsistent cortical abnormalities in major depressive disorder (MDD). Despite genetic influences on MDD and the brain, it is unclear how genetic risk for MDD is translated into spatially patterned cortical vulnerability. Here, we initially examined voxel-wise differences in cortical function and structure using the largest multi-modal MRI data from 1660 MDD patients and 1341 controls. Combined with the Allen Human Brain Atlas, we then adopted transcription-neuroimaging spatial correlation and the newly developed ensemble-based gene category enrichment analysis to identify gene categories with expression related to cortical changes in MDD. Results showed that patients had relatively circumscribed impairments in local functional properties and broadly distributed disruptions in global functional connectivity, consistently characterized by hyper-function in associative areas and hypo-function in primary regions. Moreover, the local functional alterations were correlated with genes enriched for biological functions related to MDD in general (e.g., endoplasmic reticulum stress, mitogen-activated protein kinase, histone acetylation, and DNA methylation); and the global functional connectivity changes were associated with not only MDD-general, but also brain-relevant genes (e.g., neuron, synapse, axon, glial cell, and neurotransmitters). Our findings may provide important insights into the transcriptomic signatures of regional cortical vulnerability to MDD.

Major depressive disorder (MDD) is a common, severe, disabling mental disorder that affects millions of people of all ages worldwide[1–3]. While substantial progress in the domain of psychiatry has been made over the past decades, the etiology of MDD is still largely elusive. With continuing improvements in the precision of brain imaging techniques, it is increasingly feasible to use this tool to in vivo study brain function and structure in unprecedented detail. In this context, a wealth of evidence from magnetic resonance imaging (MRI) studies has established the presence of cortical functional and structural abnormalities in MDD[4–24], by adopting the most commonly used functional measurements including amplitude of low-frequency fluctuations (ALFF, indexing local spontaneous neural activity strength)[25], regional homogeneity (ReHo, reflecting local functional

A full list of affiliations appears at the end of the paper. *A list of authors and their affiliations appears at the end of the paper.
✉e-mail: cjr.yuyongqiang@vip.163.com

synchronization degree)[26], and graph-based degree centrality (DC, characterizing global functional connectivity)[27,28] derived from resting-state functional MRI (rs-fMRI) as well as by applying voxel-based morphometry (VBM) approach to structural MRI to obtain gray matter volume (GMV)[29]. However, these previous investigations have produced inconsistent findings, which may be partially due to limited statistical power from relatively small samples. Notably, a large-scale study has examined ALFF, ReHo, and DC abnormalities in MDD by comparing 848 patients and 794 controls in the REST-meta-MDD project by the Depression Imaging REsearch ConsorTium (DIRECT) in China[30–32]. Despite this effort, independent replication in a much larger sample using more elaborate methodologies correcting for potential biases (e.g., site effects) is greatly needed to help reconcile these heterogeneous neuroimaging reports, which may refine our understanding of the neuropathology underlying MDD.

MDD has modest heritability estimated at ~40%[33–35]. Large-scale human genome-wide association studies (GWAS) have found a range of risk variants, genes, and gene sets in relation to MDD[36–41]. By use of transcriptomic profiling, moreover, Gandal et al. demonstrated that subjects with MDD had brain gene expression changes[42], yielding an updated framework for our thinking regarding how genetic variants interact with epigenetic and environmental risk factors in the brain to confer risk for MDD. In parallel, numerous neuroimaging genetics studies have documented that genetic variations influence cortical function and structure[43–48], which may contribute to predisposition to mental disorders. Despite these important findings, our knowledge about how genetic risk translates into the spatial pattern of altered cortical function and structure in MDD remains sparse. Clarifying factors that shape regional cortical vulnerability to genetic risk would help to advance the translational medicine of MDD.

The current availability of whole-brain, genome-wide expression atlases, such as the Allen Human Brain Atlas (AHBA)[49], has created new opportunities to unravel the microscale molecular substrates underlying macroscale cortical organization. This correspondence can be achieved by examining the spatial correlations between gene expression patterns and regional variations in cortical phenotypes measured by neuroimaging techniques[50–60], including functional and structural abnormalities in MDD[61–67]. Instead of making inference on thousands of genes directly as well as for the sake of facilitating biological interpretation, gene category enrichment analysis (GCEA) is typically pursued to identify functional gene categories that drive these multi-scale relationships based on gene-to-category annotation systems like the Gene Ontology (GO)[68]. Nevertheless, conventional GCEA methodology is affected by substantial false-positive biases introduced by within-category gene-gene co-expression and strong spatial autocorrelation, such that nearby cortical regions show more similar profiles of gene expression and neural phenotypes than distant regions[53,54]. These methodological challenges call for new sophisticated methods to permit more valid and interpretable inference of GCEA. In response, more recent work from Fulcher and colleagues develops a flexible ensemble-based null model that can account for the effects of gene co-expression and spatial autocorrelation[69]. This ensemble-based framework has the advantage of overcoming false-positive gene category enrichment, and thus allows researchers to better interpret the results of applying GCEA to spatially embedded transcriptional data and cortical phenotypes.

The objective of the present study was to investigate the transcriptomic signatures of regional cortical vulnerability to MDD. To realize this goal, we initially examined voxel-wise differences in cortical ALFF, ReHo, DC, and GMV using the largest multi-modal MRI data from 1660 MDD patients and 1341 healthy controls collected by the DIRECT consortium. In combination with the AHBA dataset, we then adopted transcription-neuroimaging spatial correlation and the newly developed ensemble-based GCEA to identify GO categories with gene expression related to cortical functional and structural changes in MDD patients. A schematic overview of the study design and analysis pipeline is shown in Fig. 1.

Results

Cortical functional and structural differences between MDD patients and healthy controls

The data quality control procedure brought the final sample to 1571 MDD patients and 1309 healthy controls. Demographic and clinical characteristics of the samples across 23 sites are shown in Fig. 2 (for more details see Supplementary Table 1). Overall, our voxel-wise group comparison analyses revealed a complex pattern of hyper-function and hypo-function as well as cortical atrophy in MDD patients (Fig. 3 and Supplementary Tables 2–5). With respect to cortical functional measurements, MDD patients exhibited increased ALFF in the bilateral inferior temporal gyrus, right dorsolateral prefrontal cortex and right precentral gyrus, and decreased ALFF in the bilateral medial occipital cortex relative to healthy controls ($P < 0.05$, cluster-level family-wise error [FWE] corrected) (Fig. 3A and Supplementary Table 2). Compared with controls, patients manifested increased ReHo in the left dorsomedial prefrontal cortex, left dorsolateral prefrontal cortex, bilateral inferior temporal gyrus and bilateral parahippocampal gyrus, and reduced ReHo in the bilateral medial occipital cortex, bilateral lateral occipital cortex and bilateral precentral/postcentral gyrus ($P < 0.05$, cluster-level FWE corrected) (Fig. 3B and Supplementary Table 3). In MDD patients, the pattern of DC alterations was similar to that of ReHo changes, but the spatial extent was much larger. That said, patients presented with increased DC across widespread areas including the bilateral prefrontal cortex, bilateral insula, bilateral temporal cortex, bilateral fusiform gyrus, bilateral parahippocampal gyrus and right inferior parietal lobule, and decreased DC in the bilateral occipital cortex and bilateral precentral/postcentral gyrus ($P < 0.05$, cluster-level FWE corrected) (Fig. 3C and Supplementary Table 4). With regard to cortical structure, MDD patients showed decreased GMV in the left medial prefrontal cortex and bilateral insula and operculum ($P < 0.05$, cluster-level FWE corrected) (Fig. 3D and Supplementary Table 5).

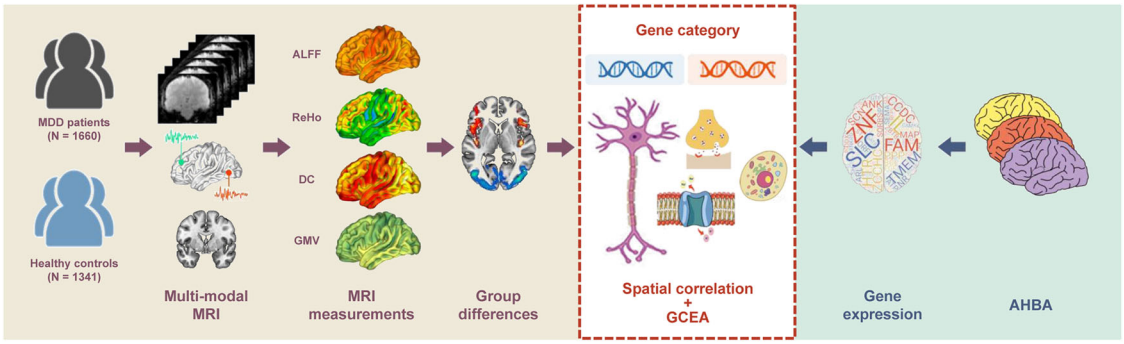

Fig. 1 | A schematic overview of the study design and analysis pipeline. Abbreviations: MDD major depressive disorder, MRI magnetic resonance imaging, ALFF amplitude of low-frequency fluctuations, ReHo regional homogeneity, DC degree centrality, GMV gray matter volume, GCEA gene category enrichment analysis, AHBA Allen Human Brain Atlas. This image and every element of this image was created by J.Z.

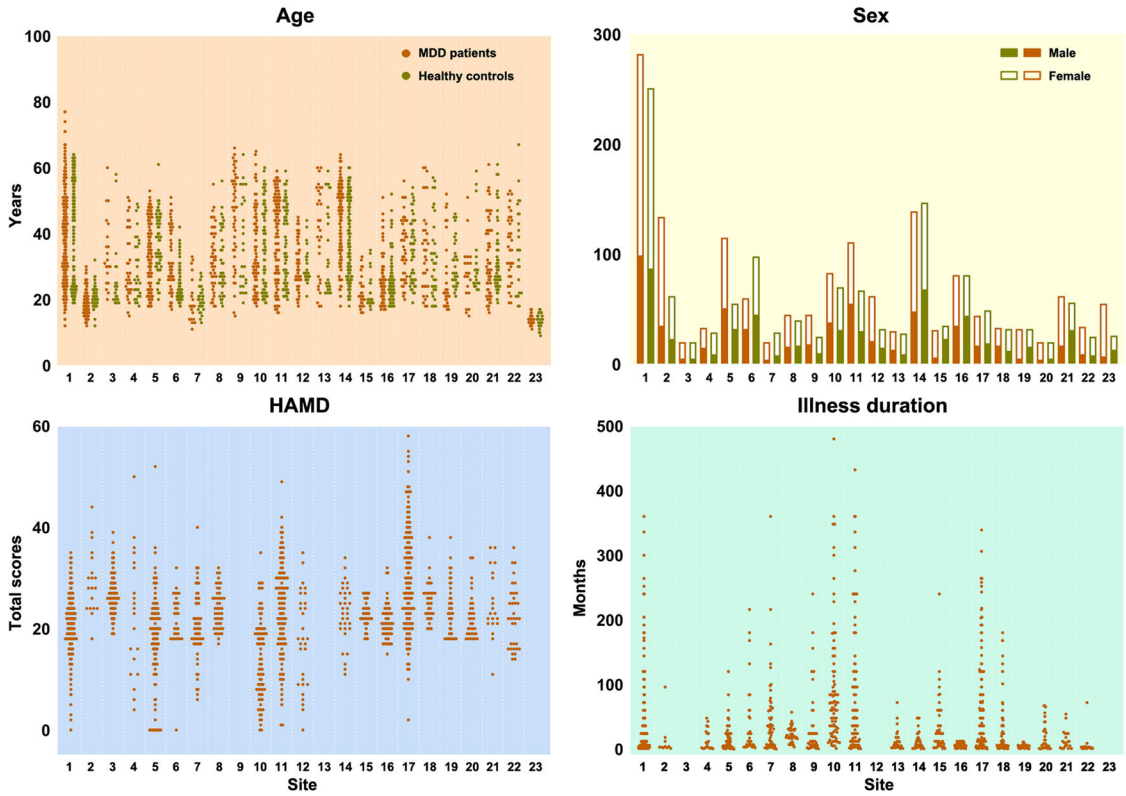

Fig. 2 | Demographic and clinical characteristics of the samples across 23 sites. Abbreviations: MDD major depressive disorder, HAMD Hamilton rating scale for depression.

Gene categories associated with cortical functional and structural changes in MDD

A combination of transcription-neuroimaging spatial correlation and the ensemble-based GCEA revealed that ALFF changes in MDD were negatively correlated with expression measures of genes enriched for GO categories involving endoplasmic reticulum (ER) stress, mitogen-activated protein kinase (MAPK), and natural killer (NK) cell (Fig. 4A and Supplementary Data 1). ReHo changes were negatively associated with gene expression of GO categories implicating histone acetylation, DNA methylation, glucose metabolism, and vascular endothelial growth factor (VEGF) (Fig. 4B and Supplementary Data 2), which are related to MDD in general. Besides their negative relations to the identical MDD-general GO categories (Fig. 4C and Supplementary Data 3), DC changes were also positively associated with gene expression of a range of brain-relevant GO categories involving neuron, synapse, axon, glial cell, and neurotransmitters such as serotonin and glutamate (Fig. 4D and Supplementary Data 3). However, there were no significant spatial correlations between MDD-related GMV changes and any GO categories.

Discussion

Our neuroimaging data represent a large, multi-site effort to examine cortical functional and structural abnormalities in MDD. With respect to functional measurements, MDD patients showed an overall consistent pattern of increase in higher-order, transmodal associative areas subserving cognition and emotion as well as decrease in lower-order, unimodal primary regions with sensory and motor functions. However, the nature and spatial extent of changes differed across these functional measurements, with ALFF and ReHo in a relatively localized fashion and DC in a widely distributed manner. Further transcription-neuroimaging spatial correlation, coupled with the ensemble-based GCEA, revealed that ALFF, ReHo, and DC changes in MDD were negatively correlated with genes enriched for some biological functions related to MDD in general; and there were also positive correlations between DC changes and many brain-relevant biological functions. As to cortical structure, however, MDD patients exhibited cortical atrophy in the medial prefrontal cortex and insula, which was not associated with any gene categories.

The current observation of hyper-function in transmodal associative areas and hypo-function in unimodal primary regions in MDD is largely coherent with prior rs-fMRI investigations and meta-analyses[5,6,11,18,70–72], especially with the earlier large-scale effort comparing 848 patients and 794 controls in the REST-meta-MDD project[32]. The finding of cortical atrophy in the medial prefrontal cortex and insula is also coincident with previous reports[13,15,16,20–24,73,74]. Moreover, the largest sample size could increase statistical power and stabilize effect estimates, which is a primary advantage of the present study given the inherent noisiness of neuroimaging data and the high heterogeneity of MDD. This advantage may enhance our confidence in interpreting our findings, which may reconcile prior heterogeneous neuroimaging reports. Various functional measurements from brain rs-fMRI have been widely employed to study psychiatric disorders[75]. We adopted three most commonly used functional measurements (ALFF, ReHo, and DC) to capture distinct yet complementary aspects of cortical functional abnormalities in MDD. ALFF measures the total power of the BOLD signal in the low-frequency range[25], thus indexing local spontaneous neural activity strength. ReHo assesses the relationship between a given voxel and its nearby voxels[26], thereby reflecting local functional synchronization degree. DC is a graph theory measure that evaluates the resting-state functional connectivity of each voxel with all other voxels across the whole brain[27,28], frequently characterizing global functional connectivity. Our findings of localized ALFF and ReHo changes and widespread DC alterations suggest that disruptions in global functional connectivity are more prominent than impairments in local functional properties in the brains of patients with MDD, endorsing the dysconnectivity hypothesis of this disorder. Notably, our results revealed an overlap between hyper-function and cortical atrophy in the medial prefrontal cortex and insula. In light of the evidence that brain function is typically shaped and constrained by the underlying anatomy[76–78], a possible explanation is that structural

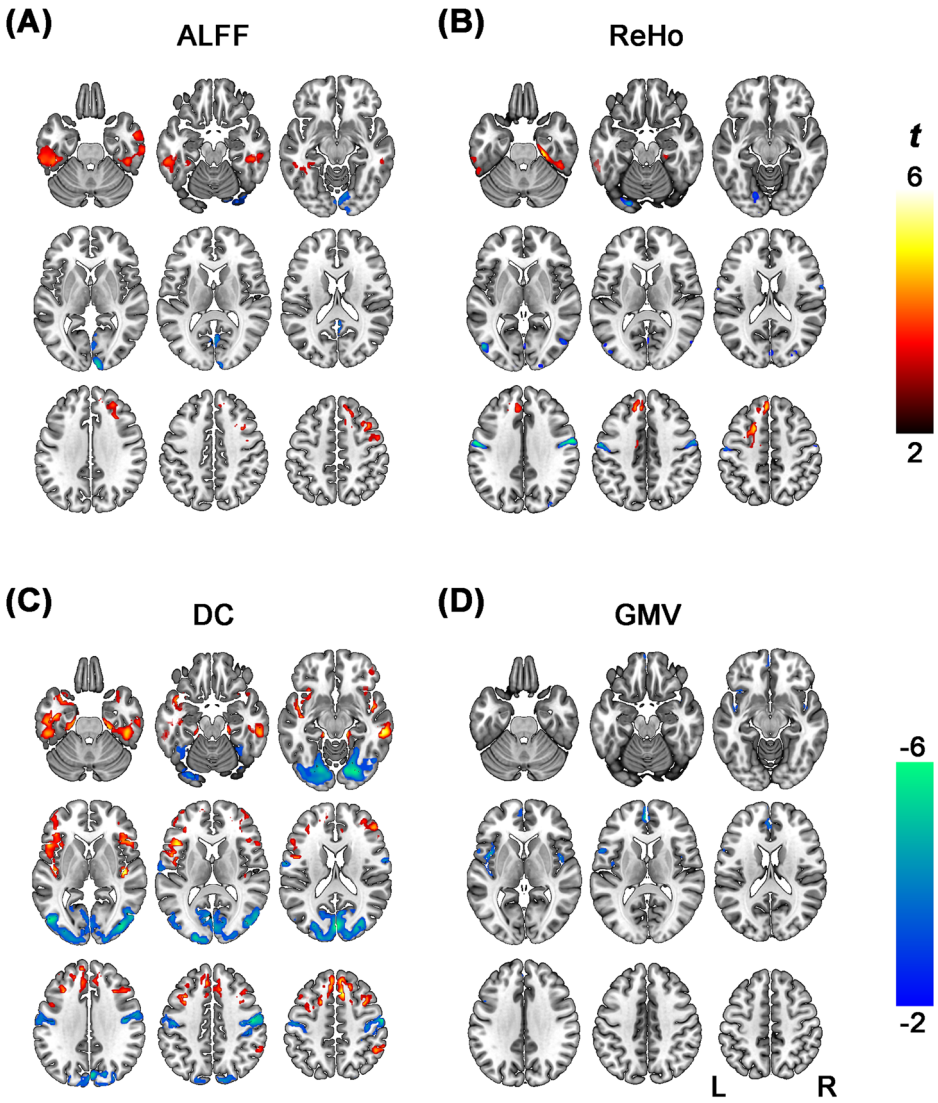

Fig. 3 | Cortical functional and structural differences between MDD patients and healthy controls. There was a mix of increased and decreased ALFF (**A**), ReHo (**B**), and DC (**C**) as well as reduced GMV (**D**) in MDD patients relative to controls ($P < 0.05$, cluster-level FWE corrected). Warm and cold colors respectively denote increase and decrease in imaging measurements in patients. Abbreviations: ALFF amplitude of low-frequency fluctuations, ReHo regional homogeneity, DC degree centrality, GMV gray matter volume, MDD major depressive disorder, FWE family-wise error.

impairment could potentially affect the function of the implicated brain regions. However, we cannot rule out the possibility that structural damage may be followed by functional reorganization, reflecting a compensatory neuroadaptive mechanism in MDD.

Further transcription-neuroimaging spatial correlation, in conjunction with the newly developed ensemble-based GCEA, showed that ALFF changes in MDD were negatively correlated with expression measures of genes enriched for GO categories involving ER stress, MAPK, and NK cell. The ER is an important organelle implicated in multiple biological processes, particularly the synthesis, folding, maturation and transport of proteins. ER dysregulation can be triggered by internal and external factors, resulting in the accumulation of unfolded and misfolded proteins in the ER lumen, referred to as ER stress. Several clinical and preclinical studies have shown a strong relationship between ER stress and depression[79,80]. To restore ER homeostasis and prevent apoptosis, the adaptive unfolded protein response (UPR) mechanism is activated[81], which is observable in patients with MDD[82]. More recent research suggests that UPR signaling pathway activation in astrocytes may serve as a novel target for antidepressant drugs[83], emphasizing the importance of ER stress in the potential therapeutic strategies for MDD. The MAPK is an essential family of serine/threonine protein kinases, which function to regulate cellular growth, differentiation, and survival in proliferative cells. Increasing evidence supports a pivotal role of the MAPK, in particular the extracellular signal-regulated kinase (ERK) subclass of MAPKs, in the pathogenesis, symptomatology, and treatment of depression[84]. In both depressed humans and animals, the ERK signaling has been found to be significantly downregulated in the prefrontal cortex and hippocampus, core brain regions implicated in depression[85,86]. Direct inhibition of the ERK pathway in the brain can induce depression-like behavior[87]. There is also empirical evidence that a variety of antidepressants exert their effects in part via normalizing the downregulated ERK activity[88–90]. It is well established that MDD is reliably associated with a reduction of NK cell activity[91,92]. A large-scale gene expression study demonstrated that the genes downregulated in MDD patients were enriched for NK cell pathways[93]. These previous reports, taken with our finding of the association between local neural activity changes and NK cell-related genes, are largely consistent with the immune dysregulation hypothesis of MDD[94].

ReHo and DC changes in MDD were negatively associated with gene expression of GO categories implicating histone acetylation, DNA methylation, glucose metabolism, and VEGF. Dynamic acetylation and deacetylation of histone lysine residues control the packing of genomic DNA, thereby influencing DNA replication, transcription, DNA repair, and cell cycle progression[95]. Recent studies have documented that histone acetylation may occur in the human brain in response to severely stressful events, resulting in transcriptional changes and the development of MDD[96]. In clinical settings, histone acetylation status has been considered a potential diagnostic biomarker for depression, while inhibitors of histone deacetylases have garnered interest as novel therapeutics[97]. DNA methylation is a process in which a methyl group is added to the nucleotide base pair cytosine where

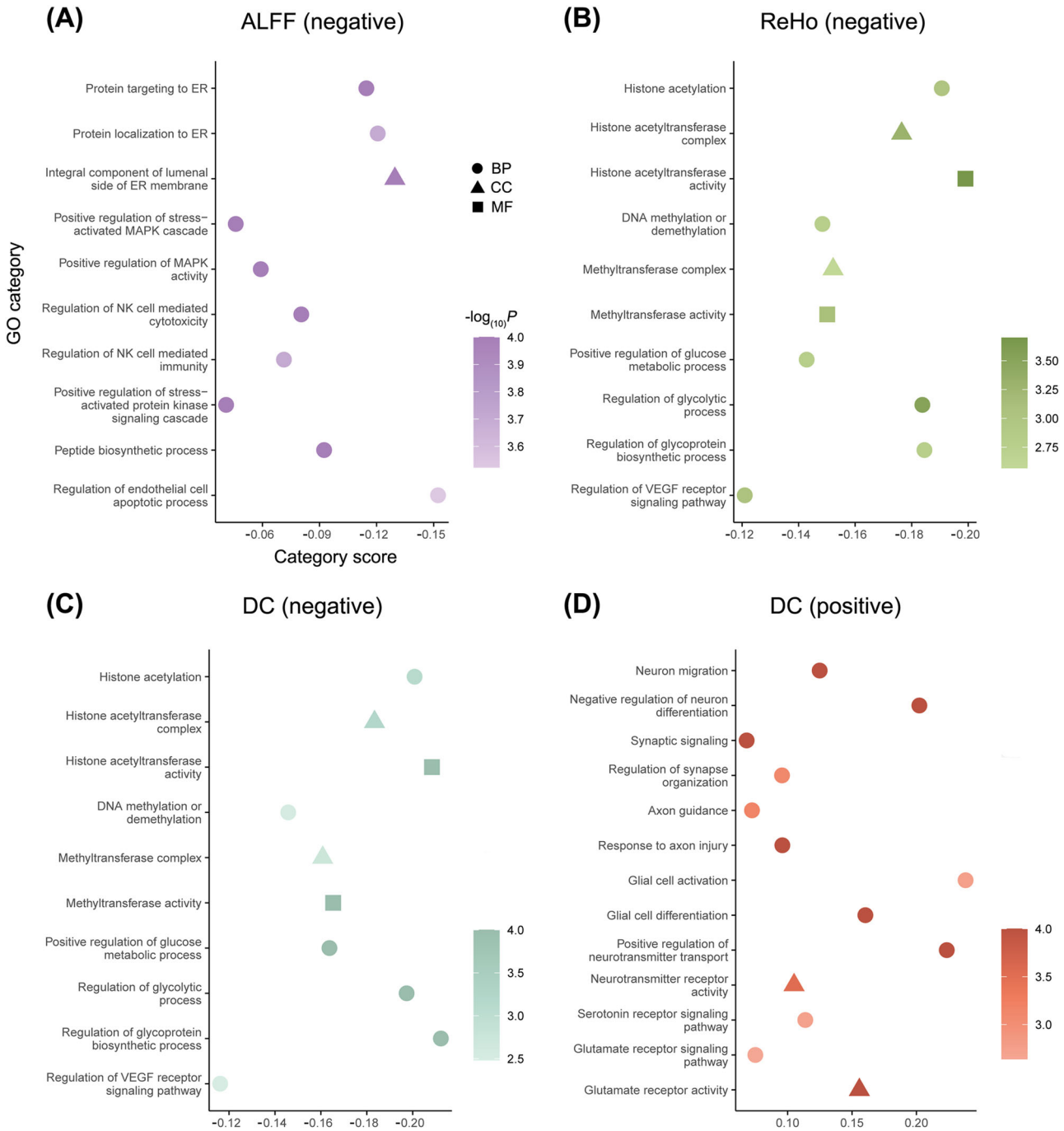

Fig. 4 | Gene categories associated with cortical functional changes in MDD. A combination of transcription-neuroimaging spatial correlation and the ensemble-based GCEA revealed that ALFF (**A**) and ReHo (**B**) changes were negatively correlated with MDD-general GO categories; DC changes were negatively associated with MDD-general GO categories (**C**) and positively associated with brain-relevant GO categories (**D**). Abbreviations: ALFF amplitude of low-frequency fluctuations, ReHo regional homogeneity, DC degree centrality, GO gene ontology, BP biological process, CC cellular component, MF molecular function, ER endoplasmic reticulum, MAPK mitogen-activated protein kinase, NK natural killer, VEGF vascular endothelial growth factor, MDD major depressive disorder, GCEA gene category enrichment analysis.

it is found next to a guanine, a region of the gene referred to as a CpG site[98]. DNA methylation can drive sustained changes in gene expression, such as gene silencing and active gene transcription. There is convergent evidence that DNA methylation modifications are associated with the etiology of depression[99–101]. Although less consistent, the relationship between antidepressant treatment and DNA methylation of several genes has also been reported[101]. These findings indicating significant contributions of histone acetylation and DNA methylation to MDD jointly advance our understanding of the epigenetic mechanisms of depression and antidepressant action[102]. Additionally, extensive research has established impaired cerebral glucose metabolism in patients with MDD[103–105]. Glycogen synthase kinase-3 (GSK-3), originally described as a negative regulator of glycogen synthesis, is a molecular hub linking numerous signaling pathways in a cell. This multifaceted protein has been suggested to be engaged in the pathogenesis of MDD, and to act as an emerging target and/or modifier of antidepressants' action[106,107]. VEGF is an angiogenic cytokine as well as a neurotrophic factor, critically involved in neurogenesis, neuroprotection, synaptic transmission, neuronal development regulation, and the differentiation and formation of

vessels in the brain[108–110]. Numerous studies have demonstrated that MDD is linked to VEGF-related gene polymorphisms, elevated blood VEGF levels, and high VEGF mRNA expression[111–113], highlighting the important role of VEGF in the pathophysiology of depression and antidepressant action of therapeutic interventions.

Contrasting with ReHo alterations showing no positive correlations with any GO categories, DC changes were positively associated with gene expression of a range of brain-relevant GO categories involving neuron, synapse, axon, glial cell, and neurotransmitters such as serotonin and glutamate, which are all key components of the cerebral cortex. On the one hand, global functional connectivity is crucial for the effective segregation and integration of information processing in the brain. Neural communication that underlies global functional connectivity is largely dependent on the integrity of these essential cortical components. On the other hand, solid evidence shows that MDD is associated with abnormalities in neuron[114], synapse[115], axon[116], and glial cell[117]. The relationship between serotonin dysfunction and MDD has been arguably the most well-characterized, giving rise to the serotonin hypothesis of depression[118]. Prior work has also suggested that glutamate neurotransmitter deficits may contribute to altered connectivity and network function in the brains of depressed patients[119], which might be reversed by novel treatments[120]. Combined, our findings work jointly to favor the notion that widespread disruptions in global functional connectivity are a more prominent neural characteristic of MDD, which may be modulated by a complex interaction of polygenes involving not only MDD-general, but also brain-relevant biological functions.

Our neuroimaging data from large, multi-site Chinese Han samples add to the human brain mapping literature on MDD, which is typically skewed towards western samples. This is a major strength of the present study, but our results must be viewed in light of some limitations. First, the clinical complexity of MDD together with the differences in patient populations, scanners, and study protocols across sites may have biased our results. Here, appropriate and specific methodologies (e.g., ComBat harmonization) were adopted to rule out the possible effects of these confounding factors. Second, the brain gene expression data were derived from six post-mortem donors devoid of MDD and of non-Chinese ethnicity, whereas the neuroimaging data were obtained from MDD patients and healthy controls of Chinese ethnicity. These differences were ignored during the transcriptome-neuroimaging spatial correlation analyses. The inter-individual variability should be captured and considered in future work. Third, we focused our analyses solely on the cerebral cortex and excluded subcortical regions. The relationship between gene expression and subcortical abnormalities in MDD will be part of our future investigations. Fourth, our transcriptome-neuroimaging spatial correlation analyses were performed on four cortical MRI measurements separately. Additional correction for the number of the cortical MRI measurements yielded no significant correlations. Therefore, we reported the results that only corrected the number of gene categories as type II error control is equally important in exploratory research. Fifth, we found no genetic associations with cortical atrophy in MDD. This may be due to the use of GMV, which could confound effects specific to cortical thickness or surface area. As these structural measures have been shown to be genetically and phenotypically independent[121], cortical thickness and surface area should be further examined in future studies. Finally, although the AHBA dataset offers an excellent resource to allow researchers to examine transcription-neuroimaging spatial correlations, future experimental animal studies are needed to validate and interpret our findings.

In conclusion, our large-scale neuroimaging data demonstrated that MDD patients had relatively circumscribed impairments in local functional properties (ALFF and ReHo) and broadly distributed disruptions in global functional connectivity (DC). These cortical functional abnormalities were consistently characterized by hyper-function in transmodal associative areas and hypo-function in unimodal primary regions. Moreover, transcription-neuroimaging spatial correlation revealed that the local functional alterations were correlated with MDD-general genes; and the global functional connectivity changes were associated with not only MDD-general, but also brain-relevant genes. Apart from helping reconcile prior heterogeneous neuroimaging reports, our findings may provide important insights into the transcriptomic signatures of regional cortical vulnerability to MDD.

Methods

Participants

A total of 1660 MDD patients and 1341 healthy controls were recruited by twenty-three research groups from the DIRECT consortium. The studies were approved by local Institutional Review Boards, and written informed consent was obtained from all participants. All ethical regulations relevant to human research participants were followed. Participants were excluded if they had no information on age or sex. Both groups had demographic features including age, sex and education. For MDD patients, clinical characteristics included onset age, illness duration, first-episode or recurrent status, episode number, medication use, 17-item Hamilton Rating Scale for Depression (HAMD), and Hamilton Rating Scale for Anxiety (HAMA).

Image acquisition and quality control

Details of MRI acquisition parameters across 23 sites can be found in Supplementary Table 6. Image quality control was performed by a well-trained researcher (J.Z.) who had previous expertise in inspecting neuroimaging data. For functional data, all the images were visually inspected to exclude those with visible artifacts (e.g., ghosting artifacts, metal artifacts, susceptibility artifacts, and blooming artifacts) and incomplete brain coverage. During fMRI preprocessing, we additionally excluded the images with excessive head motion during fMRI scanning (i.e., translational or rotational motion > 3 mm or 3 °) and bad spatial normalization. For structural data, manual quality control strategies are considered the current gold standard for quality control, although several options for automated quality control (e.g., Euler number) have provided potential time efficient and reproducible alternatives[122]. Therefore, we adopted two manual quality control strategies for the structural MRI images: (1) visual inspection with exclusion of visible artifacts, organic brain abnormality and inaccurate segmentation, and (2) visual inspection with manual editing where the inaccurate segmentation was manually edited. The quality control procedure brought the final sample to 1571 MDD patients and 1309 healthy controls. Demographic and clinical characteristics of the samples across 23 sites are shown in Fig. 2 (for more details see Supplementary Table 1). With the participants pooled together, we found that the two groups were comparable on age, but patients were preferentially female and had a lower educational level relative to controls (see Supplementary Table 7 for detailed information).

Image preprocessing

The preprocessing of rs-fMRI data was conducted using the toolbox for Data Processing & Analysis for Brain Imaging on Surface (DPABISurf)[123], which is based on fMRIPrep[124], FreeSurfer[125], ANTs[126], FSL[127], AFNI[128], SPM[129], PALM[130], dcm2niix[131], GNU Parallel[132], MATLAB (The MathWorks Inc., Natick, MA, US), Docker (https://docker.com), and DPABI[133]. The preprocessing pipeline included: (i) discarding the initial 10 time points; (ii) converting data into BIDS format[134]; (iii) calling fMRIPrep 20.2.1 docker; (iv) conducting anatomical data processing as follows: the T1-weighted image was corrected for intensity nonuniformity using N4BiasFieldCorrection[135]; the corrected T1-weighted image was then skull-stripped with ANTs; fast (FSL 5.0.9)[136] was adopted to segment brain tissue into gray matter (GM), white matter (WM), and cerebrospinal fluid (CSF); recon -all (FreeSurfer 6.0.1) was used to reconstruct brain surfaces; ANTs-derived brain masks and FreeSurfer-derived segmentations of the cortical GM were reconciled using a custom variation of the method of Mindboggle[137]; nonlinear registration with antsRegistration (ANTs 2.3.3) was performed for the volume-based spatial normalization to one standard space (MNI152NLin2009cAsym)[138] using brain-extracted versions of both T1-weighted reference and the T1-weighted template. (v) Functional data preprocessing was conducted as follows: a blood-oxygen-level-dependent (BOLD) reference volume and its skull-stripped version were generated using a custom methodology of fMRIPrep. The BOLD reference was then co-registered to the T1-weighted

reference using bbregister (FreeSurfer)[139]. Head motion parameters with respect to the BOLD reference (transformation matrices, and six corresponding rotation and translation parameters) were estimated using mcflirt (FSL 5.0.9). BOLD volumes were slice-time corrected using 3dTshift from AFNI. Next, the functional datasets were normalized to the MNI152N-Lin2009cAsym standard space using the deformation parameters estimated during the anatomical data preprocessing. Several confounding time courses were calculated and regressed out from the data: the estimated head motion parameters based on the Friston-24 model[140], the linear drift, DVARS, and BOLD signals of the WM and CSF. In addition, Jenkinson frame-wise displacement (FD) was computed as relative root mean square displacement between time points[127], and mean FD was used to address the residual effects of motion in subsequent group-level statistical analyses. Finally, the functional datasets were band-pass filtered in a frequency range of 0.01 to 0.1 Hz.

Cortical MRI measurements and statistical analysis

To calculate ALFF, a Fast Fourier Transform was initially performed to transform the BOLD time courses into a frequency domain and obtained the power spectrum. ALFF was defined as the averaged square root of the power spectrum in a specific low-frequency band (0.01–0.1 Hz)[25]. ReHo was computed as the Kendall's coefficient of concordance (KCC) of the time course of a given voxel with those of its nearest neighbors (26 voxels)[26]. To compute DC, we first calculated Pearson's correlation coefficients between the BOLD time courses of all pairs of voxels within the whole brain and obtained the whole brain functional connectivity matrix. For a given voxel, DC was defined as the sum of positive functional connectivity above a threshold of 0.25 between that voxel and all other voxels across the whole brain[27,28]. Finally, GMV was derived from the FSL-fast segmentation of the T1-weighted images during the anatomical data processing.

The resultant ALFF, ReHo, DC, and GMV maps were spatially smoothed with a Gaussian kernel of $6 \times 6 \times 6$ mm^3 full-width at half maximum. For the purpose of standardization, the value of each voxel in the ALFF, ReHo, and DC maps was divided by the respective global mean value, yielding standardized ALFF, ReHo, and DC maps. To reduce potential biases and non-biological variability induced by site effects, we applied ComBat[141], a harmonization technique previously shown to successfully remove site effects in multi-modal imaging measurements[142–144], to the ALFF, ReHo, DC, and GMV maps. ComBat harmonization approach makes use of a multivariate linear mixed effects regression with terms for biological variables and site to model imaging measurements. In this framework, empirical Bayes methods are adopted to improve the estimation of the model parameters for small samples. Note that we included group, age, and sex as covariates in the ComBat model to preserve important biological trends in the data and avoid overcorrection. After these procedures, cortical ALFF, ReHo, DC, and GMV differences between 1571 MDD patients and 1309 healthy controls were examined using two-sample *t*-tests in a voxel-wise manner, with age and sex as nuisance covariates for GMV and mean FD as an additional covariate for ALFF, ReHo, and DC. The statistical analyses generated four t maps for ALFF, ReHo, DC, and GMV, representing inter-group differences in these imaging measurements. Multiple comparisons were corrected using the cluster-level FWE method, resulting in a cluster defining threshold of $P < 0.001$ and a corrected cluster significance of $P < 0.05$, following current standard[145].

Cortical gene expression data processing

Brain gene expression data were obtained from the downloadable AHBA dataset (http://www.brain-map.org)[49,146]. The dataset was derived from six human post-mortem donors (Supplementary Table 8). The original expression data of more than 20000 genes at 3702 spatially distinct brain tissue samples were processed using a newly proposed pipeline[54]. Specifically, we first updated the probe-to-gene annotations based on the latest available information from the National Center for Biotechnology Information (NCBI) using the Re-Annotator package[147]. With intensity-based filtering, we excluded probes that did not exceed the background noise in at least 50% of samples across all donors. As multiple probes were used to measure the expression level of a single gene, we further used the RNA-seq data as a reference to select probes. After removing genes that do not overlap between RNA-seq and microarray datasets, we computed the correlations between microarray and RNA-seq expression measures for the remaining genes. After excluding probes with low correlations ($r < 0.2$), a representative probe for a gene was selected based on the highest correlation to the RNA-seq data. Here, only the tissue samples in the left cerebral cortex were included. For one, all six donors had expression data in the left hemisphere, whereas only two donors had samples in the right hemisphere. For another, the inclusion of subcortical samples might introduce potential biases given the considerable differences in gene expression between cortical and subcortical regions[49]. To account for potential between-sample differences and donor-specific effects in gene expression, we conducted both within-sample cross-gene and within-gene cross-sample normalization by using the scaled robust sigmoid normalization method. Differential stability (DS) is a measure of consistent regional variation across donor brains. Previous research has reported that genes with high DS scores demonstrate more consistent spatial expression patterns between donors[146]. As gene expression conservation across subjects is a prerequisite for the transcription-neuroimaging spatial correlations, we only selected genes with relatively more conserved expression patterns for analysis. To achieve this goal, we ranked the genes by their DS values and chose the genes with the top 50% highest DS for the main analysis. After these processing procedures, we obtained normalized expression data of 5013 genes for 1280 tissue samples. To ensure accuracy, we further focused our analyses on the tissue samples within a cerebral cortical gray matter mask, generating a final sample × gene matrix of 753 × 5013.

Transcription-neuroimaging spatial correlation and gene category enrichment analysis

To derive group differences in imaging measurements of the above-mentioned 753 tissue samples, we drew a spherical region (radius = 2 mm) centered at the MNI coordinate of each sample and extracted the average t-value of voxels within the sphere from the statistical t maps for ALFF, ReHo, DC, and GMV, respectively. Then, cross-sample (753 samples) Pearson's correlations between gene expression and t-values were performed in a gene-wise manner (5013 genes), yielding 5013 spatial correlation coefficients (henceforth referred to as gene scores). In accordance with the Fulcher et al. study[69], we conducted neuroimaging-spatial ensemble-based GCEA for these gene scores in the following way. First, updated GO term hierarchy and annotation files were obtained from the GO (http://geneontology.org/) on 11th July 2022. Second, direct gene-to-category annotations were performed for the 5013 AHBA genes, and we restricted our analyses to GO categories with 10–200 annotations. Third, the gene scores were agglomerated at the level of GO categories as a mean score of genes annotated to each GO category. Fourth, we adopted the brainSMASH toolbox (https://github.com/murraylab/brainsmash), based on the spatial-lag model[148], to generate 10,000 surrogate maps with spatial autocorrelation matched to that of the ALFF, ReHo, DC, and GMV t maps, respectively. Fifth, spatial correlations between gene expression and the 10,000 spatial autocorrelation-preserving surrogate maps were carried out to construct a null distribution (i.e., neuroimaging-spatial ensemble-based null model) of mean gene scores for each GO category. Finally, statistical significance of a GO category was assessed by comparing the GO category score derived from the real data to the neuroimaging-spatial ensemble-based null. The significance level was set at two-sided$P < 0.05$ (i.e., higher or lower than the null), Benjamini-Hochberg false discovery rate (FDR) corrected for multiple testing.

Statistics and reproducibility

All statistical tests used, the sample sizes, the number of replicates, and how replicates were defined are described in the corresponding methods.

Reporting summary

Further information on research design is available in the Nature Portfolio Reporting Summary linked to this article.

Data availability

The neuroimaging data that support the findings and the accession codes for the transcriptomic data are publicly available in the study's Open Science Framework repository (https://osf.io/76qnk/). Brain gene expression data are obtained from the AHBA dataset (https://human.brain-map.org/static/download). All other data are available from the corresponding author on reasonable request.

Received: 17 January 2024; Accepted: 31 July 2024;
Published online: 08 August 2024

References

1. Malhi, G. S. & Mann, J. J. Depression. *Lancet* **392**, 2299–2312 (2018).
2. Alexopoulos, G. S. Depression in the elderly. *Lancet* **365**, 1961–1970 (2005).
3. Thapar, A., Eyre, O., Patel, V. & Brent, D. Depression in young people. *Lancet* **400**, 617–631 (2022).
4. Zheng, R. et al. Abnormal voxel-wise whole-brain functional connectivity in first-episode, drug-naive adolescents with major depression disorder. *Eur. Child Adolesc. Psychiatry,* https://doi.org/10.1007/s00787-022-01959-y (2022).
5. Yuan, J. et al. Altered spontaneous brain activity in major depressive disorder: An activation likelihood estimation meta-analysis. *J. Affect. Disord.* **314**, 19–26 (2022).
6. Gong, J. et al. Common and distinct patterns of intrinsic brain activity alterations in major depression and bipolar disorder: voxel-based meta-analysis. *Transl. Psychiatry* **10**, 353 (2020).
7. Gray, J. P., Muller, V. I., Eickhoff, S. B. & Fox, P. T. Multimodal abnormalities of brain structure and function in major depressive disorder: a meta-analysis of neuroimaging studies. *Am. J. Psychiatry* **177**, 422–434 (2020).
8. Zhao, W. et al. The reduction of vitamin D in females with major depressive disorder is associated with worse cognition mediated by abnormal brain functional connectivity. *Prog. Neuropsychopharmacol. Biol. Psychiatry* **118**, 110577 (2022).
9. Hao, H., Chen, C., Mao, W., Zhong, J. & Dai, Z. Aberrant brain regional homogeneity in first-episode drug-naive patients with major depressive disorder: a voxel-wise meta-analysis. *J. Affect. Disord.* **245**, 63–71 (2019).
10. Shi, Y. et al. Abnormal functional connectivity strength in first-episode, drug-naive adult patients with major depressive disorder. *Prog. Neuropsychopharmacol. Biol. Psychiatry* **97**, 109759 (2020).
11. Zhou, M. et al. Intrinsic cerebral activity at resting state in adults with major depressive disorder: a meta-analysis. *Prog. Neuropsychopharmacol. Biol. Psychiatry* **75**, 157–164 (2017).
12. Sheng, J. et al. Spatiotemporal, metabolic, and therapeutic characterization of altered functional connectivity in major depressive disorder. *Hum. Brain Mapp.* **39**, 1957–1971 (2018).
13. Zhang, H. et al. Brain gray matter alterations in first episodes of depression: a meta-analysis of whole-brain studies. *Neurosci. Biobehav. Rev.* **60**, 43–50 (2016).
14. Li, W. et al. Characterization of brain blood flow and the amplitude of low-frequency fluctuations in major depressive disorder: a multimodal meta-analysis. *J. Affect. Disord.* **210**, 303–311 (2017).
15. Arnone, D. et al. Computational meta-analysis of statistical parametric maps in major depression. *Hum. Brain Mapp.* **37**, 1393–1404 (2016).
16. Peng, W., Chen, Z., Yin, L., Jia, Z. & Gong, Q. Essential brain structural alterations in major depressive disorder: a voxel-wise meta-analysis on first episode, medication-naive patients. *J. Affect. Disord.* **199**, 114–123 (2016).
17. Chen, Z. Q. et al. Voxel-wise meta-analyses of brain blood flow and local synchrony abnormalities in medication-free patients with major depressive disorder. *J. Psychiatry Neurosci.* **40**, 401–411 (2015).
18. Iwabuchi, S. J. et al. Localized connectivity in depression: a meta-analysis of resting state functional imaging studies. *Neurosci. Biobehav. Rev.* **51**, 77–86 (2015).
19. Zhao, Y. J. et al. Brain grey matter abnormalities in medication-free patients with major depressive disorder: a meta-analysis. *Psychol. Med.* **44**, 2927–2937 (2014).
20. Du, M. et al. Brain grey matter volume alterations in late-life depression. *J. Psychiatry Neurosci.* **39**, 397–406 (2014).
21. Bora, E., Fornito, A., Pantelis, C. & Yucel, M. Gray matter abnormalities in major depressive disorder: a meta-analysis of voxel based morphometry studies. *J. Affect. Disord.* **138**, 9–18 (2012).
22. Lai, C. H. Gray matter volume in major depressive disorder: a meta-analysis of voxel-based morphometry studies. *Psychiatry Res.* **211**, 37–46 (2013).
23. Zheng, R., Zhang, Y., Yang, Z., Han, S. & Cheng, J. Reduced brain gray matter volume in patients with first-episode major depressive disorder: a quantitative meta-analysis. *Front Psychiatry* **12**, 671348 (2021).
24. Serra-Blasco, M. et al. Structural brain correlates in major depression, anxiety disorders and post-traumatic stress disorder: a voxel-based morphometry meta-analysis. *Neurosci. Biobehav. Rev.* **129**, 269–281 (2021).
25. Zang, Y. F. et al. Altered baseline brain activity in children with ADHD revealed by resting-state functional MRI. *Brain Dev.* **29**, 83–91 (2007).
26. Zang, Y., Jiang, T., Lu, Y., He, Y. & Tian, L. Regional homogeneity approach to fMRI data analysis. *Neuroimage* **22**, 394–400 (2004).
27. Zhu, J. et al. Altered coupling between resting-state cerebral blood flow and functional connectivity in Schizophrenia. *Schizophr. Bull.* **43**, 1363–1374 (2017).
28. Tomasi, D. & Volkow, N. D. Functional connectivity hubs in the human brain. *Neuroimage* **57**, 908–917 (2011).
29. Ashburner, J. & Friston, K. J. Voxel-based morphometry-the methods. *Neuroimage* **11**, 805–821 (2000).
30. Chen, X. et al. The complexity of functional connectivity profiles of the subgenual anterior cingulate cortex and dorsal lateral prefrontal cortex in major depressive disorder: a DIRECT Consortium Study. *bioRxiv*, 2023.2003.2009.531726, https://doi.org/10.1101/2023.03.09.531726 (2023).
31. Chen, X. et al. The DIRECT consortium and the REST-meta-MDD project: towards neuroimaging biomarkers of major depressive disorder. *Psychoradiology* **2**, 32–42 (2022).
32. Yan, C. G. et al. Reduced default mode network functional connectivity in patients with recurrent major depressive disorder. *Proc. Natl Acad. Sci. USA* **116**, 9078–9083 (2019).
33. Corfield, E. C., Yang, Y., Martin, N. G. & Nyholt, D. R. A continuum of genetic liability for minor and major depression. *Transl. Psychiatry* **7**, e1131 (2017).
34. Sullivan, P. F., Neale, M. C. & Kendler, K. S. Genetic epidemiology of major depression: review and meta-analysis. *Am. J. Psychiatry* **157**, 1552–1562 (2000).
35. Flint, J. & Kendler, K. S. The genetics of major depression. *Neuron* **81**, 484–503 (2014).
36. Wray, N. R. et al. Genome-wide association analyses identify 44 risk variants and refine the genetic architecture of major depression. *Nat. Genet.* **50**, 668–681 (2018).
37. Howard, D. M. et al. Genome-wide association study of depression phenotypes in UK Biobank identifies variants in excitatory synaptic pathways. *Nat. Commun.* **9**, 1470 (2018).
38. Howard, D. M. et al. Genome-wide meta-analysis of depression identifies 102 independent variants and highlights the importance of the prefrontal brain regions. *Nat. Neurosci.* **22**, 343–352 (2019).
39. Consortium, C. Sparse whole-genome sequencing identifies two loci for major depressive disorder. *Nature* **523**, 588–591 (2015).

40. Hyde, C. L. et al. Identification of 15 genetic loci associated with risk of major depression in individuals of European descent. *Nat. Genet.* **48**, 1031–1036 (2016).
41. Ripke, S. et al. A mega-analysis of genome-wide association studies for major depressive disorder. *Mol. Psychiatry* **18**, 497–511 (2013).
42. Gandal, M. J. et al. Shared molecular neuropathology across major psychiatric disorders parallels polygenic overlap. *Science* **359**, 693–697 (2018).
43. Hibar, D. P. et al. Common genetic variants influence human subcortical brain structures. *Nature* **520**, 224–229 (2015).
44. Zhao, B. et al. Common variants contribute to intrinsic human brain functional networks. *Nat. Genet.* **54**, 508–517 (2022).
45. Grasby, K. L. et al. The genetic architecture of the human cerebral cortex. *Science* **367**, https://doi.org/10.1126/science.aay6690 (2020).
46. Sun, B. B. et al. Genetic map of regional sulcal morphology in the human brain from UK biobank data. *Nat. Commun.* **13**, 6071 (2022).
47. Elliott, L. T. et al. Genome-wide association studies of brain imaging phenotypes in UK Biobank. *Nature* **562**, 210–216 (2018).
48. Stein, J. L. et al. Identification of common variants associated with human hippocampal and intracranial volumes. *Nat. Genet.* **44**, 552–561 (2012).
49. Hawrylycz, M. J. et al. An anatomically comprehensive atlas of the adult human brain transcriptome. *Nature* **489**, 391–399 (2012).
50. Liu, S. et al. Frequency-dependent genetic modulation of neuronal oscillations: a combined transcriptome and resting-state functional MRI study. *Cereb. Cortex* **32**, 5132–5144 (2022).
51. Zhang, C. et al. Genetic architecture underlying differential resting-state functional connectivity of subregions within the human visual cortex. *Cereb. Cortex* **32**, 2063–2078 (2022).
52. Chen, J. et al. Molecular basis underlying functional connectivity of fusiform gyrus subregions: a transcriptome-neuroimaging spatial correlation study. *Cortex* **152**, 59–73 (2022).
53. Fornito, A., Arnatkeviciute, A. & Fulcher, B. D. Bridging the gap between connectome and transcriptome. *Trends Cogn. Sci.* **23**, 34–50 (2019).
54. Arnatkeviciute, A., Fulcher, B. D. & Fornito, A. A practical guide to linking brain-wide gene expression and neuroimaging data. *Neuroimage* **189**, 353–367 (2019).
55. Shen, Y. et al. Transcriptional substrates underlying functional connectivity profiles of subregions within the human sensorimotor cortex. *Hum. Brain Mapp.* **43**, 5562–5578 (2022).
56. Xu, X. et al. Genetic mechanisms underlying gray matter volume changes in patients with drug-naive first-episode schizophrenia. *Cereb. Cortex* **33**, 2328–2341 (2023).
57. Zhao, H. et al. Genetic mechanisms underlying brain functional homotopy: a combined transcriptome and resting-state functional MRI study. *Cereb. Cortex* **33**, 3387–3400 (2023).
58. Li, Q. et al. Resting-state brain functional alterations and their genetic mechanisms in drug-naive first-episode psychosis. *Schizophrenia* **9**, 13 (2023).
59. Huang, W. et al. Neural correlates of early-life urbanization and their spatial relationships with gene expression, neurotransmitter, and behavioral domain atlases. *Mol. Neurobiol.* https://doi.org/10.1007/s12035-024-03962-7 (2024).
60. Cui, S. et al. Molecular mechanisms underlying resting-state brain functional correlates of behavioral inhibition. *Neuroimage* **283**, 120415 (2023).
61. Althubaity, N. et al. Choroid plexus enlargement is associated with neuroinflammation and reduction of blood brain barrier permeability in depression. *Neuroimage Clin.* **33**, 102926 (2022).
62. Li, J. et al. Cortical structural differences in major depressive disorder correlate with cell type-specific transcriptional signatures. *Nat. Commun.* **12**, 1647 (2021).
63. Anderson, K. M. et al. Convergent molecular, cellular, and cortical neuroimaging signatures of major depressive disorder. *Proc. Natl Acad. Sci. USA* **117**, 25138–25149 (2020).
64. Xue, K. et al. Local dynamic spontaneous brain activity changes in first-episode, treatment-naive patients with major depressive disorder and their associated gene expression profiles. *Psychol. Med*. 1–10, https://doi.org/10.1017/S0033291720003876 (2020).
65. Xue, K. et al. Transcriptional signatures of the cortical morphometric similarity network gradient in first-episode, treatment-naive major depressive disorder. *Neuropsychopharmacology*, https://doi.org/10.1038/s41386-022-01474-3 (2022).
66. Fang, Q. et al. Transcriptional substrates of brain structural and functional impairments in drug-naive first-episode patients with major depressive disorder. *J. Affect. Disord.* **325**, 522–533 (2023).
67. Sun, X. et al. Cerebral blood flow changes and their genetic mechanisms in major depressive disorder: a combined neuroimaging and transcriptome study. *Psychol. Med.* https://doi.org/10.1017/S0033291722003750 (2023).
68. Ashburner, M. et al. Gene ontology: tool for the unification of biology. The Gene Ontology Consortium. *Nat. Genet.* **25**, 25–29 (2000).
69. Fulcher, B. D., Arnatkeviciute, A. & Fornito, A. Overcoming false-positive gene-category enrichment in the analysis of spatially resolved transcriptomic brain atlas data. *Nat. Commun.* **12**, 2669 (2021).
70. Zhuo, C. et al. Different spatial patterns of brain atrophy and global functional connectivity impairments in major depressive disorder. *Brain Imaging Behav.* **11**, 1678–1689 (2017).
71. Zhu, J., Lin, X., Lin, C. & Zhuo, C. Distance-dependent alterations in local functional connectivity in drug-naive major depressive disorder. *Psychiatry Res. Neuroimag.* **270**, 80–85 (2017).
72. Wang, L. et al. The effects of antidepressant treatment on resting-state functional brain networks in patients with major depressive disorder. *Hum. Brain Mapp.* **36**, 768–778 (2015).
73. Sacher, J. et al. Mapping the depressed brain: a meta-analysis of structural and functional alterations in major depressive disorder. *J. Affect. Disord.* **140**, 142–148 (2012).
74. Du, M. Y. et al. Voxelwise meta-analysis of gray matter reduction in major depressive disorder. *Prog. Neuropsychopharmacol. Biol. Psychiatry* **36**, 11–16 (2012).
75. Canario, E., Chen, D. & Biswal, B. A review of resting-state fMRI and its use to examine psychiatric disorders. *Psychoradiology* **1**, 42–53 (2021).
76. Honey, C. J., Kotter, R., Breakspear, M. & Sporns, O. Network structure of cerebral cortex shapes functional connectivity on multiple time scales. *Proc. Natl Acad. Sci. USA* **104**, 10240–10245 (2007).
77. Honey, C. J. et al. Predicting human resting-state functional connectivity from structural connectivity. *Proc. Natl Acad. Sci. USA* **106**, 2035–2040 (2009).
78. Suarez, L. E., Markello, R. D., Betzel, R. F. & Misic, B. Linking structure and function in macroscale brain networks. *Trends Cogn. Sci.* **24**, 302–315 (2020).
79. Mao, J., Hu, Y., Ruan, L., Ji, Y. & Lou, Z. Role of endoplasmic reticulum stress in depression (Review). *Mol. Med. Rep.* **20**, 4774–4780 (2019).
80. Xiang, C., Wang, Y., Zhang, H. & Han, F. The role of endoplasmic reticulum stress in neurodegenerative disease. *Apoptosis: Int. J. Program. Cell Death* **22**, 1–26 (2017).
81. Ron, D. & Walter, P. Signal integration in the endoplasmic reticulum unfolded protein response. *Nat. Rev. Mol. Cell Biol.* **8**, 519–529 (2007).
82. Kowalczyk, M. et al. Cellular response to unfolded proteins in depression. *Life* **11**, https://doi.org/10.3390/life11121376 (2021).
83. Jozwiak-Bebenista, M. et al. The importance of endoplasmic reticulum stress as a novel antidepressant drug target and its

potential impact on CNS disorders. *Pharmaceutics* **14**, https://doi.org/10.3390/pharmaceutics14040846 (2022).
84. Wang, J. Q. & Mao, L. The ERK pathway: molecular mechanisms and treatment of depression. *Mol. Neurobiol.* **56**, 6197–6205 (2019).
85. Qi, X., Lin, W., Li, J., Pan, Y. & Wang, W. The depressive-like behaviors are correlated with decreased phosphorylation of mitogen-activated protein kinases in rat brain following chronic forced swim stress. *Behav. Brain Res.* **175**, 233–240 (2006).
86. Dwivedi, Y. et al. Reduced activation and expression of ERK1/2 MAP kinase in the post-mortem brain of depressed suicide subjects. *J. Neurochem.* **77**, 916–928 (2001).
87. Qi, X. et al. A role for the extracellular signal-regulated kinase signal pathway in depressive-like behavior. *Behav. Brain Res.* **199**, 203–209 (2009).
88. First, M. et al. The effects of fluoxetine treatment in a chronic mild stress rat model on depression-related behavior, brain neurotrophins and ERK expression. *J. Mol. Neurosci. MN* **45**, 246–255 (2011).
89. Qi, X. et al. Fluoxetine increases the activity of the ERK-CREB signal system and alleviates the depressive-like behavior in rats exposed to chronic forced swim stress. *Neurobiol. Dis.* **31**, 278–285 (2008).
90. Gourley, S. L. et al. Regionally specific regulation of ERK MAP kinase in a model of antidepressant-sensitive chronic depression. *Biol. Psychiatry* **63**, 353–359 (2008).
91. Pike, J. L. & Irwin, M. R. Dissociation of inflammatory markers and natural killer cell activity in major depressive disorder. *Brain Behav. Immun.* **20**, 169–174 (2006).
92. Zorrilla, E. P. et al. The relationship of depression and stressors to immunological assays: a meta-analytic review. *Brain Behav. Immun.* **15**, 199–226 (2001).
93. Jansen, R. et al. Gene expression in major depressive disorder. *Mol. Psychiatry* **21**, 339–347 (2016).
94. Blume, J., Douglas, S. D. & Evans, D. L. Immune suppression and immune activation in depression. *Brain Behav. Immun.* **25**, 221–229 (2011).
95. Wade, P. A., Pruss, D. & Wolffe, A. P. Histone acetylation: chromatin in action. *Trends Biochem. Sci.* **22**, 128–132 (1997).
96. Wu, M. S. et al. Effects of histone modification in major depressive disorder. *Curr. Neuropharmacol.* **20**, 1261–1277 (2022).
97. Park, H. S., Kim, J., Ahn, S. H. & Ryu, H. Y. Epigenetic targeting of histone deacetylases in diagnostics and treatment of depression. *Int. J. Mol. Sci.* **22**, https://doi.org/10.3390/ijms22105398 (2021).
98. Meaney, M. J. Epigenetics and the biological definition of gene x environment interactions. *Child Dev.* **81**, 41–79 (2010).
99. Story Jovanova, O. et al. DNA methylation signatures of depressive symptoms in middle-aged and elderly persons: meta-analysis of multiethnic epigenome-wide studies. *JAMA Psychiatry* **75**, 949–959, (2018).
100. Clark, S. L. et al. A methylation study of long-term depression risk. *Mol. Psychiatry* **25**, 1334–1343 (2020).
101. Li, M. et al. What do DNA methylation studies tell us about depression? A systematic review. *Transl. Psychiatry* **9**, 68 (2019).
102. Vialou, V., Feng, J., Robison, A. J. & Nestler, E. J. Epigenetic mechanisms of depression and antidepressant action. *Annu. Rev. Pharmacol. Toxicol.* **53**, 59–87 (2013).
103. Su, L. et al. Cerebral metabolism in major depressive disorder: a voxel-based meta-analysis of positron emission tomography studies. *BMC Psychiatry* **14**, 321 (2014).
104. Ernst, J. et al. Increased pregenual anterior cingulate glucose and lactate concentrations in major depressive disorder. *Mol. Psychiatry* **22**, 113–119 (2017).
105. Li, C. T., Su, T. P., Wang, S. J., Tu, P. C. & Hsieh, J. C. Prefrontal glucose metabolism in medication-resistant major depression. *Br. J. Psychiatry* **206**, 316–323 (2015).
106. McCallum, R. T. & Perreault, M. L. Glycogen Synthase Kinase-3: a focal point for advancing pathogenic inflammation in depression. *Cells* **10**, https://doi.org/10.3390/cells10092270 (2021).
107. Duda, P., Hajka, D., Wojcicka, O., Rakus, D. & Gizak, A. GSK3beta: a master player in depressive disorder pathogenesis and treatment responsiveness. *Cells* **9**, https://doi.org/10.3390/cells9030727 (2020).
108. Nowacka, M. M. & Obuchowicz, E. Vascular endothelial growth factor (VEGF) and its role in the central nervous system: a new element in the neurotrophic hypothesis of antidepressant drug action. *Neuropeptides* **46**, 1–10 (2012).
109. Jin, K. et al. Vascular endothelial growth factor (VEGF) stimulates neurogenesis in vitro and in vivo. *Proc. Natl Acad. Sci. USA* **99**, 11946–11950 (2002).
110. Storkebaum, E., Lambrechts, D. & Carmeliet, P. VEGF: once regarded as a specific angiogenic factor, now implicated in neuroprotection. *BioEssays: N. Rev. Mol., Cell. Develop. Biol.* **26**, 943–954 (2004).
111. Tseng, P. T., Cheng, Y. S., Chen, Y. W., Wu, C. K. & Lin, P. Y. Increased levels of vascular endothelial growth factor in patients with major depressive disorder: a meta-analysis. *Eur. Neuropsychopharmacol.* **25**, 1622–1630 (2015).
112. Sharma, A. N., da Costa e Silva, B. F., Soares, J. C., Carvalho, A. F. & Quevedo, J. Role of trophic factors GDNF, IGF-1 and VEGF in major depressive disorder: a comprehensive review of human studies. *J. Affect. Disord.* **197**, 9–20 (2016).
113. Xie, T. et al. VEGF-related polymorphisms identified by GWAS and risk for major depression. *Transl. Psychiatry* **7**, e1055 (2017).
114. Tye, K. M. et al. Dopamine neurons modulate neural encoding and expression of depression-related behaviour. *Nature* **493**, 537–541 (2013).
115. Thompson, S. M. Plasticity of synapses and reward circuit function in the genesis and treatment of depression. *Neuropsychopharmacology* **48**, 90–103 (2023).
116. Williams, M. R. et al. Axonal myelin increase in the callosal genu in depression but not schizophrenia. *Psychol. Med.* **45**, 2145–2155 (2015).
117. Kim, Y. K. & Na, K. S. Role of glutamate receptors and glial cells in the pathophysiology of treatment-resistant depression. *Prog. Neuropsychopharmacol. Biol. Psychiatry* **70**, 117–126 (2016).
118. Moncrieff, J. et al. The serotonin theory of depression: a systematic umbrella review of the evidence. *Mol. Psychiatry* https://doi.org/10.1038/s41380-022-01661-0 (2022).
119. Duman, R. S., Sanacora, G. & Krystal, J. H. Altered connectivity in depression: GABA and glutamate neurotransmitter deficits and reversal by novel treatments. *Neuron* **102**, 75–90 (2019).
120. Murrough, J. W., Abdallah, C. G. & Mathew, S. J. Targeting glutamate signalling in depression: progress and prospects. *Nat. Rev. Drug Discov.* **16**, 472–486 (2017).
121. Winkler, A. M. et al. Cortical thickness or grey matter volume? The importance of selecting the phenotype for imaging genetics studies. *Neuroimage* **53**, 1135–1146 (2010).
122. Monereo-Sanchez, J. et al. Quality control strategies for brain MRI segmentation and parcellation: practical approaches and recommendations—insights from the Maastricht study. *Neuroimage* **237**, 118174 (2021).
123. Yan, C.-G., Wang, X.-D. & Lu, B. DPABISurf: data processing & analysis for brain imaging on surface. *Sci. Bull.* **66**, 2453–2455 (2021).
124. Esteban, O. et al. fMRIPrep: a robust preprocessing pipeline for functional MRI. *Nat. Methods* **16**, 111–116 (2019).
125. Dale, A. M., Fischl, B. & Sereno, M. I. Cortical surface-based analysis. I. Segmentation and surface reconstruction. *Neuroimage* **9**, 179–194 (1999).
126. Avants, B. B., Tustison, N. & Song, G. Advanced normalization tools (ANTS). *Insight J.* **2**, 1–35 (2009).

127. Jenkinson, M., Bannister, P., Brady, M. & Smith, S. Improved optimization for the robust and accurate linear registration and motion correction of brain images. *Neuroimage* **17**, 825–841 (2002).
128. Cox, R. W. & Hyde, J. S. Software tools for analysis and visualization of fMRI data. *NMR Biomed.* **10**, 171–178 (1997).
129. Ashburner, J. SPM: a history. *Neuroimage* **62**, 791–800 (2012).
130. Winkler, A. M., Ridgway, G. R., Webster, M. A., Smith, S. M. & Nichols, T. E. Permutation inference for the general linear model. *Neuroimage* **92**, 381–397 (2014).
131. Li, X., Morgan, P. S., Ashburner, J., Smith, J. & Rorden, C. The first step for neuroimaging data analysis: DICOM to NIfTI conversion. *J. Neurosci. Methods* **264**, 47–56 (2016).
132. Tange, O. Gnu parallel-the command-line power tool. *USENIX Mag.* **36**, 42–47 (2011).
133. Yan, C. G., Wang, X. D., Zuo, X. N. & Zang, Y. F. DPABI: data processing & analysis for (resting-state) brain imaging. *Neuroinformatics* **14**, 339–351 (2016).
134. Gorgolewski, K. J. et al. The brain imaging data structure, a format for organizing and describing outputs of neuroimaging experiments. *Sci. Data* **3**, 160044 (2016).
135. Tustison, N. J. et al. N4ITK: improved N3 bias correction. *IEEE Trans. Med. Imaging* **29**, 1310–1320, (2010).
136. Zhang, Y., Brady, M. & Smith, S. Segmentation of brain MR images through a hidden Markov random field model and the expectation-maximization algorithm. *IEEE Trans. Med. Imaging* **20**, 45–57 (2001).
137. Klein, A. et al. Mindboggling morphometry of human brains. *PLoS Comput. Biol.* **13**, e1005350 (2017).
138. Fonov, V. S., Evans, A. C., McKinstry, R. C., Almli, C. R. & Collins, D. Unbiased nonlinear average age-appropriate brain templates from birth to adulthood. *Neuroimage* **47**, S102 (2009).
139. Greve, D. N. & Fischl, B. Accurate and robust brain image alignment using boundary-based registration. *Neuroimage* **48**, 63–72 (2009).
140. Friston, K. J., Williams, S., Howard, R., Frackowiak, R. S. & Turner, R. Movement-related effects in fMRI time-series. *Magn. Reson. Med.* **35**, 346–355 (1996).
141. Johnson, W. E., Li, C. & Rabinovic, A. Adjusting batch effects in microarray expression data using empirical Bayes methods. *Biostatistics* **8**, 118–127 (2007).
142. Fortin, J. P. et al. Harmonization of cortical thickness measurements across scanners and sites. *Neuroimage* **167**, 104–120 (2018).
143. Fortin, J. P. et al. Harmonization of multi-site diffusion tensor imaging data. *Neuroimage* **161**, 149–170 (2017).
144. Yu, M. et al. Statistical harmonization corrects site effects in functional connectivity measurements from multi-site fMRI data. *Hum. Brain Mapp.* **39**, 4213–4227 (2018).
145. Eklund, A., Nichols, T. E. & Knutsson, H. Cluster failure: Why fMRI inferences for spatial extent have inflated false-positive rates. *Proc. Natl Acad. Sci. USA* **113**, 7900–7905 (2016).
146. Hawrylycz, M. et al. Canonical genetic signatures of the adult human brain. *Nat. Neurosci.* **18**, 1832–1844 (2015).
147. Arloth, J., Bader, D. M., Roh, S. & Altmann, A. Re-Annotator: annotation pipeline for microarray probe sequences. *PLoS One* **10**, e0139516 (2015).
148. Burt, J. B., Helmer, M., Shinn, M., Anticevic, A. & Murray, J. D. Generative modeling of brain maps with spatial autocorrelation. *Neuroimage* **220**, 117038 (2020).

Acknowledgements

The study was supported by the National Natural Science Foundation of China (grant numbers: 82371928 and 82071905), the Anhui Provincial Natural Science Foundation (grant number: 2308085MH277), the Outstanding Youth Support Project of Anhui Province Universities (grant number: gxyqZD2022026), the Scientific Research Key Project of Anhui Province Universities (grant number: 2022AH051135), the Scientific Research Foundation of Anhui Medical University (grant number: 2022xkj143), and the Anhui University Collaborative Innovation Project (grant number: GXXT-2021-065). We thank the Allen Institute for Brain Science founders and staff who supplied the brain expression data.

Author contributions

Jiajia Zhu performed the analyses and wrote the initial manuscript; Yongqiang Yu conceived the project and contributed to the editing of the manuscript; Jiajia Zhu, Xiao Chen, Bin Lu, Xue-Ying Li, Zi-Han Wang, Li-Ping Cao, Guan-Mao Chen, Jian-Shan Chen, Tao Chen, Tao-Lin Chen, Yu-Qi Cheng, Zhao-Song Chu, Shi-Xian Cui, Xi-Long Cui, Zhao-Yu Deng, Qi-Yong Gong, Wen-Bin Guo, Can-Can He, Zheng-Jia-Yi Hu, Qian Huang, Xin-Lei Ji, Feng-Nan Jia, Li Kuang, Bao-Juan Li, Feng Li, Hui-Xian Li, Tao Li, Tao Lian, Yi-Fan Liao, Xiao-Yun Liu, Yan-Song Liu, Zhe-Ning Liu, Yi-Cheng Long, Jian-Ping Lu, Jiang Qiu, Xiao-Xiao Shan, Tian-Mei Si, Peng-Feng Sun, Chuan-Yue Wang, Hua-Ning Wang, Xiang Wang, Ying Wang, Yu-Wei Wang, Xiao-Ping Wu, Xin-Ran Wu, Yan-Kun Wu, Chun-Ming Xie, Guang-Rong Xie, Peng Xie, Xiu-Feng Xu, Zhen-Peng Xue, Hong Yang, Hua Yu, Min-Lan Yuan, Yong-Gui Yuan, Ai-Xia Zhang, Jing-Ping Zhao, Ke-Rang Zhang, Wei Zhang, Zi-Jing Zhang, Chao-Gan Yan, the DIRECT Consortium, and Yongqiang Yu were involved in data collection and processing.

Competing interests

The authors declare no competing interests.

Additional information

Supplementary information The online version contains supplementary material available at https://doi.org/10.1038/s42003-024-06665-w.

Correspondence and requests for materials should be addressed to Yongqiang Yu.

Peer review information *Communications Biology* thanks Anna Fiorito and the other, anonymous, reviewer(s) for their contribution to the peer review of this work. Primary Handling Editors: Mary Teena Joy and Joao Valente.

[1]Department of Radiology, The First Affiliated Hospital of Anhui Medical University, Hefei 230022, China. [2]Research Center of Clinical Medical Imaging, Anhui Province Hefei 230032, China. [3]Anhui Provincial Institute of Translational Medicine, Hefei 230032, China. [4]CAS Key Laboratory of Behavioral Science, Institute of Psychology, Chinese Academy of Sciences, Beijing 100101, China. [5]International Big-Data Center for Depression Research, Chinese Academy of Sciences, Beijing 100101, China. [6]Magnetic Resonance Imaging Research Center, Institute of Psychology, Chinese Academy of Sciences, Beijing 100101, China. [7]Department of Psychology, University of Chinese Academy of Sciences, Beijing 100049, China. [8]Affiliated Brain Hospital of Guangzhou Medical University, Guangzhou 510370, China. [9]The First Affiliated Hospital of Jinan University, Guangzhou, Guangdong 250024, China. [10]Department of Radiology, The First Affiliated Hospital, College of Medicine, Zhejiang University, Hangzhou, Zhejiang 310058, China. [11]Huaxi MR Research Center (HMRRC), Department of Radiology, West China Hospital of Sichuan University, Chengdu, Sichuan 610044, China. [12]Research Unit of Psychoradiology, Chinese Academy of Medical Sciences, Chengdu, Sichuan 610052, China. [13]Department of Psychiatry, First Affiliated Hospital of Kunming Medical University, Kunming, Yunnan 650032, China. [14]Sino-Danish College, University of Chinese Academy of Sciences, Beijing 101408, China. [15]Sino-Danish Center for Education and Research, Graduate University of Chinese Academy of Sciences, Beijing 101408, China. [16]Department of Psychiatry, and National Clinical Research Center for Mental Disorders, The Second Xiangya Hospital of Central South University, Changsha 410011 Hunan, China. [17]Department of Neurology, Affiliated ZhongDa Hospital of Southeast University, Nanjing, Jiangsu 210009, China. [18]Department of Psychiatry, The First Affiliated Hospital of Chongqing Medical University, Chongqing 400042, China. [19]Department of Clinical Psychology, Suzhou Psychiatric Hospital, The Affiliated Guangji Hospital of Soochow University, Suzhou, Jiangsu 215003, China. [20]Xijing Hospital of Air Force Military Medical University, Xi'an, Shaanxi 710032, China. [21]Beijing Anding Hospital, Capital Medical University, Beijing 100120, China. [22]Affiliated Mental Health Center & Hangzhou Seventh People's Hospital, Zhejiang University School of Medicine, Hangzhou, Zhejiang 310063, China. [23]Mental Health Center and Psychiatric Laboratory, West China Hospital of Sichuan University, Chengdu, Sichuan 610044, China. [24]Department of Psychosomatics and Psychiatry, Zhongda Hospital, School of Medicine, Southeast University, Nanjing, Jiangsu 210009, China. [25]Shenzhen Kangning Hospital Shenzhen, Guangzhou 518020, China. [26]Faculty of Psychology, Southwest University, Chongqing 400715, China. [27]National Clinical Research Center for Mental Disorders (Peking University Sixth Hospital) & Key Laboratory of Mental Health, Ministry of Health (Peking University), Beijing 100191, China. [28]Xi'an Central Hospital, Xi'an, Shaanxi 710004, China. [29]Institute of Neuroscience, Chongqing Medical University, Chongqing 400016, China. [30]Chongqing Key Laboratory of Neurobiology, Chongqing 400000, China. [31]Department of Neurology, The First Affiliated Hospital of Chongqing Medical University, Chongqing 400042, China. [32]West China Hospital of Sichuan University, Chengdu, Sichuan 610044, China. [33]First Hospital of Shanxi Medical University, Taiyuan, Shanxi 030001, China. ✉e-mail: cjr.yuyongqiang@vip.163.com

the DIRECT Consortium

Yongqiang Yu[1,2,3]✉, Jiajia Zhu[1,2,3], Xiao Chen[4,5,6,7], Bin Lu[4,5,6,7], Xue-Ying Li[4,5,6,7], Zi-Han Wang[4,5,6,7], Li-Ping Cao[8], Guan-Mao Chen[9], Jian-Shan Chen[8], Tao Chen[10], Tao-Lin Chen[11,12], Yu-Qi Cheng[13], Zhao-Song Chu[13], Shi-Xian Cui[4,14,15], Xi-Long Cui[16], Zhao-Yu Deng[4,5,6,7], Qi-Yong Gong[11,12], Wen-Bin Guo[16], Can-Can He[17], Zheng-Jia-Yi Hu[4,14,15], Qian Huang[18], Xin-Lei Ji[16], Feng-Nan Jia[19], Li Kuang[18], Bao-Juan Li[20], Feng Li[21], Hui-Xian Li[4,5,6,7], Tao Li[22,23], Tao Lian[4,5,6], Yi-Fan Liao[4,5,6], Xiao-Yun Liu[24], Yan-Song Liu[19], Zhe-Ning Liu[16], Yi-Cheng Long[16], Jian-Ping Lu[25], Jiang Qiu[26], Xiao-Xiao Shan[16], Tian-Mei Si[27], Peng-Feng Sun[28], Chuan-Yue Wang[21], Hua-Ning Wang[20], Xiang Wang[16], Ying Wang[9], Yu-Wei Wang[4,5,6,7], Xiao-Ping Wu[28], Xin-Ran Wu[26], Yan-Kun Wu[27], Chun-Ming Xie[17], Guang-Rong Xie[16], Peng Xie[29,30,31], Xiu-Feng Xu[13], Zhen-Peng Xue[25], Hong Yang[10], Hua Yu[22,23], Min-Lan Yuan[32], Yong-Gui Yuan[24], Ai-Xia Zhang[33], Jing-Ping Zhao[16], Ke-Rang Zhang[33], Wei Zhang[32], Zi-Jing Zhang[4,5,6] & Chao-Gan Yan[4,5,6,7,14,15]